Cerebral Cortex June 2007;17:1283–1291
doi:10.1093/cercor/bhl038
Advance Access publication July 10, 2006

Cytochrome Oxidase and Neurofilament Reactivity in Monocularly Deprived Human Primary Visual Cortex

Kevin R. Duffy[1], Kathryn M. Murphy[2], Matthew P. Frosch[3] and Margaret S. Livingstone[4]

[1]Department of Psychology, Life Sciences Centre, Dalhousie University, Halifax, Nova Scotia, Canada B3H 4J1, [2]Department of Psychology, McMaster University, Hamilton, Ontario, Canada L8S 4K1, [3]C.S. Kubik Laboratory for Neuropathology, Department of Pathology, Massachusetts General Hospital, Boston, MA 02114, USA and [4]Department of Neurobiology, Harvard Medical School, Boston, MA 02115, USA

Previous studies of human primary visual cortex (V1) have demonstrated a significant eye-specific decrease in cytochrome oxidase (CO) staining following monocular enucleation. We have extended these results by examining CO staining and neurofilament labeling in V1 from a patient with long-standing monocular blindness. A pattern of reduced neurofilament reactivity was found to align with pale CO-stained ocular dominance columns. Neurons located within deprived ocular dominance columns were significantly smaller compared with those in nondeprived columns. A spatial analysis of the relationship between CO blobs and ocular dominance columns revealed that both deprived and nondeprived blobs tended to align with the centers of ocular dominance columns.

Keywords: CO blobs, deprivation, human, neurofilament, ocular dominance columns, primary visual cortex

Introduction

The primary visual cortex (V1) of many mammals is organized into physiologically and anatomically distinct domains. Neurons within V1 can exhibit a physiologically measured graded preference for stimulation of one eye over the other (Hubel and Wiesel 1959, 1962, 1968). This feature of V1 is represented anatomically as alternating columns of neurons that preferentially connect to the left or right eye and span the thickness of the cortex (Hubel and Wiesel 1972; LeVay and others 1975). This organization of ocular dominance columns is most pronounced within layer IV and extends throughout the full tangential extent of V1, except in regions representing the monocular crescent and the blind spot.

In the supragranular layers, and less obviously in the infragranular layers, highly active neurons are grouped together into regularly spaced blobs of cortex that are surrounded by comparatively less active interblob regions (DeYoe and others 1995). The relatively more active blobs stain heavily for the enzyme cytochrome oxidase (CO) and have therefore become known as CO blobs (Livingstone and Hubel 1984; Murphy and others 1995), patches (Horton and Hubel 1981; Horton 1984), or puffs (Carroll and Wong-Riley 1984). The spatial relationship between CO blobs and ocular dominance columns varies across species. In macaque monkeys, blobs are aligned with the centers of ocular dominance columns (Horton and Hubel 1981; Horton 1984), whereas in squirrel monkeys and galagos, there is no clear spatial relationship between these cortical features (Horton and Hocking 1996; Xu and others 2005). In cats, blobs appear to be functionally eye specific but their spatial relationship to ocular dominance columns is not as precise as that seen in the macaque (Murphy and others 1995).

Neural organizations within V1 are strongly influenced by changes in visual experience. Monocular deprivation in humans and macaque monkeys can cause a reduction of CO staining within ocular dominance columns serving the deprived eye and in CO blobs that align with deprived-eye columns (Horton 1984; Horton and Hedley-Whyte 1984). In addition to metabolic changes, visual deprivation has been shown to cause a reduction in cytoskeleton protein labeling within the central visual pathway. Monocular deprivation leads to a loss of microtubule-associated protein 2 labeling (Hendry and Bhandari 1992) and nonphosphorylated neurofilament labeling (Duffy and Livingstone 2005) in deprived-eye columns of macaque monkey V1. Monocular deprivation also causes loss of nonphosphorylated neurofilament labeling in deprived-eye layers of the cat lateral geniculate nucleus (Bickford and others 1998). Proteins that compose the cytoskeleton provide intracellular scaffolding that supports neuronal structure. A change in neurofilaments could impact the integrity of circuitry that processes neural signals to enable normal visual function.

Previous studies of experience-dependent changes in cytoskeleton labeling (Hendry and Bhandari 1992; Bickford and others 1998; Duffy and Livingstone 2005) used animal models and leave open the question of whether neurofilaments in the human visual cortex are similarly affected by visual deprivation. We have examined CO staining and neurofilament labeling within human V1 from a subject with long-standing monocular visual deprivation. This work was performed to determine the impact of deprivation on CO staining and neurofilament labeling within V1 in order to gain further insight into the neural changes that result from visual deprivation in humans. In addition, the high quality of CO staining within V1 provided an opportunity to examine quantitatively the spatial relationship between human CO blobs and ocular dominance columns.

Materials and Methods

Subject

We had the opportunity to examine area V1 from the brain of an 86-year-old woman with long-standing monocular blindness. Clinical information available at the time of autopsy did not provide details regarding the duration of the monocular deprivation beyond suggesting that it was lifelong. The severity of the monocular impairment was evident on examination of the optic nerves, which revealed that the affected side was markedly reduced in volume with a glassy gray appearance. Microscopic examination confirmed the severity and chronicity of the lesion, as there was a pronounced loss of axons and myelin sheaths without any evidence of recent injury on the affected side, compared with a normal appearing contralateral optic nerve. This was further supported by the appropriate laminar transsynaptic neuronal degeneration in the lateral geniculate nuclei. Tissue collection was permitted in accordance with institutional guidelines for protection of human subjects.

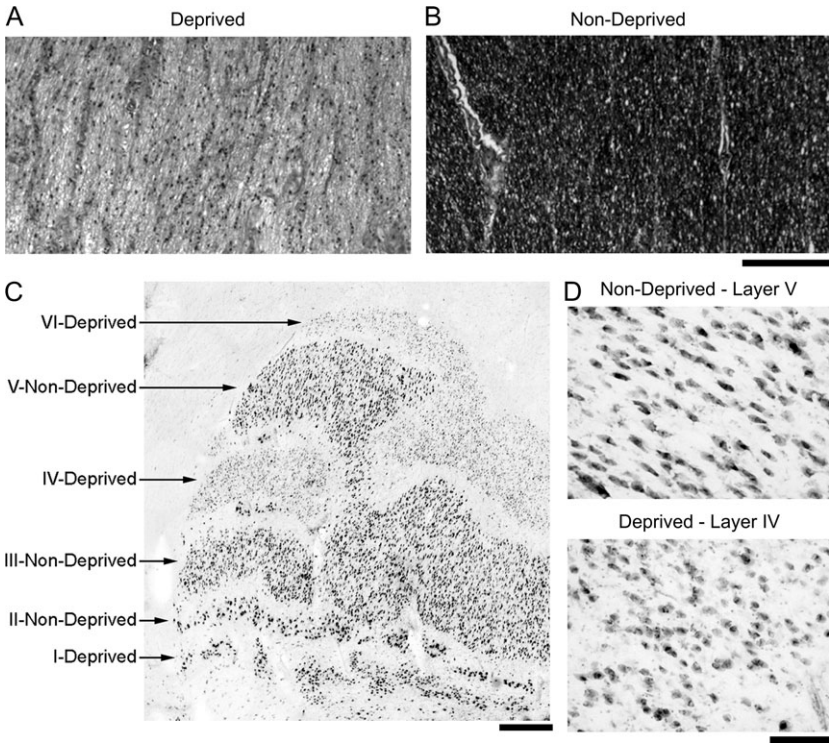

Figure 1. Images of the optic nerves (top: Luxol fast blue/H&E stain for myelin) and lateral geniculate nucleus (bottom: Nissl stain) provided support for the clinical report that the lesion was monocular (right eye) and long standing. The deprived-eye's optic nerve (*A*) was weakly stained and showed a pronounced loss of myelin compared with the contralateral optic nerve (*B*). A similar result was observed in sections from the left lateral geniculate nucleus where deprived layers were weakly stained (*C*) and, at high magnification, exhibited evidence of neuronal atrophy, with preservation of neurons in nondeprived layers (*D*). Scale bars = 250 μm (*A*, *B*), 500 μm (*C*), 100 μm (*D*).

Histology

The brain was removed from the skull shortly after death and placed in 0.1 M phosphate buffer with 4% formalin. After 2 days of fixation in formalin, V1 from the hemisphere ipsilateral to the impaired eye was dissected so that the dorsal bank of the calcarine sulcus (tissue mapping the lower visual field) could be flattened and sectioned tangential to the cortical surface. Coronal sections of V1 from the same hemisphere were cut through the lingual gyrus (representing upper visual space) and through the posterior aspect of the cuneus. Before sectioning, tissue blocks were cryoprotected at 4 °C in phosphate-buffered saline (0.1 M) with 30% sucrose for 2 days. The blocks of tissue were then cut into 50-μm-thick sections with a freezing microtome.

Sections of V1 were processed for CO, Nissl substance, or nonphosphorylated neurofilament protein so that a comparison between reaction patterns could be made. Adjacent sections were not reacted for the same marker so as to avoid double counting cells during quantification. Neurofilament labeling was performed using the antibody SMI-32 (Sternberger Monoclonals, Lutherville, MD). SMI-32 is a monoclonal antibody that identifies a nonphosphorylated epitope on heavy and medium molecular weight subunits of neurofilament protein (Lee and others 1988). Tissue sections cut for SMI-32 immunoreactivity were first placed in cold methanol with 0.3% hydrogen peroxide for 5 min and then preincubated for 1 h in Tris-buffered saline (TBS) containing 0.1% Triton X-100 and 5% normal goat serum. Sections were then incubated overnight at 4 °C in TBS containing 0.1% Triton X-100, 5% normal goat serum, and primary antibody (SMI-32; 1:2000). On the following day, immunoreactivity was revealed using a Vectastain ABC kit (Vector Laboratories, Burlingame, CA) and the chromogen 3,3′-diaminobenzidine (DAB) with peroxide. Sections were mounted onto glass slides, left overnight to dry, dehydrated in a series of graded alcohols, defatted in xylenes, and then coverslipped with DPX (BDH Labs, Poole, UK).

CO staining followed procedures described previously (Wong-Riley 1979; Horton 1984; Murphy and others 1995). Immediately after cutting, tissue sections were mounted onto gelatin-coated glass slides and air-dried overnight. Sections were then incubated at 40 °C in a mixture of phosphate buffer (0.1 M, pH 7.4), cytochrome C oxidase, catalase, and the chromogen DAB. Sections were kept in this solution until maximal contrast between CO strong and weak regions was obtained (approximately 8 h). Sections were then dehydrated in a series of graded alcohols, defatted in xylenes, and coverslipped with DPX (BDH Labs, Poole, UK).

Cell bodies in some V1 sections were revealed using thionin staining for Nissl substance. The optic nerves, in continuity with the chiasm and proximal optic tracts, were dissected free from the ventral surface of the brain, embedded in paraffin, and stained for myelin with routine Luxol fast blue/H&E methods. The lateral geniculate nuclei were examined after sectioning the fixed tissue in the coronal plane and staining for Nissl substance with thionin.

Quantification

Comparison of CO and SMI-32 reactivity in V1 was achieved by aligning adjacent tangential sections using the pattern of radial blood vessels. Ocular dominance column borders were determined from CO-stained sections through layer IV using a computer program written with Matlab 4.0 (MathWorks, Natick, MA) that plotted contours at half the maximum-to-minimum optical staining intensity within the analysis area. All measurements were made in tangential sections from the dorsal bank of the calcarine sulcus (tissue mapping the lower visual field). The density of neurofilament-labeled cells within deprived and nondeprived ocular dominance columns was calculated from 4 nonoverlapping regions within layer IVB, each approximately 15 mm^2. Only cells with distinct perikaryal labeling were included in our analysis. Neurofilament-labeled cell density within deprived and nondeprived columns was statistically compared using a paired student's *t*-test. Ocular dominance column widths were measured in CO-stained sections, and the differences between the deprived and nondeprived column widths were compared using a paired student's *t*-test.

The soma area, numeric density, and optical staining intensity of neurons in deprived and nondeprived regions of V1 were measured from a Nissl-stained section using a compound microscope (20× objective) and image analysis software (Image-Pro Plus, Media Cybernetics, San Diego, CA). The Nissl section selected for sampling was cut

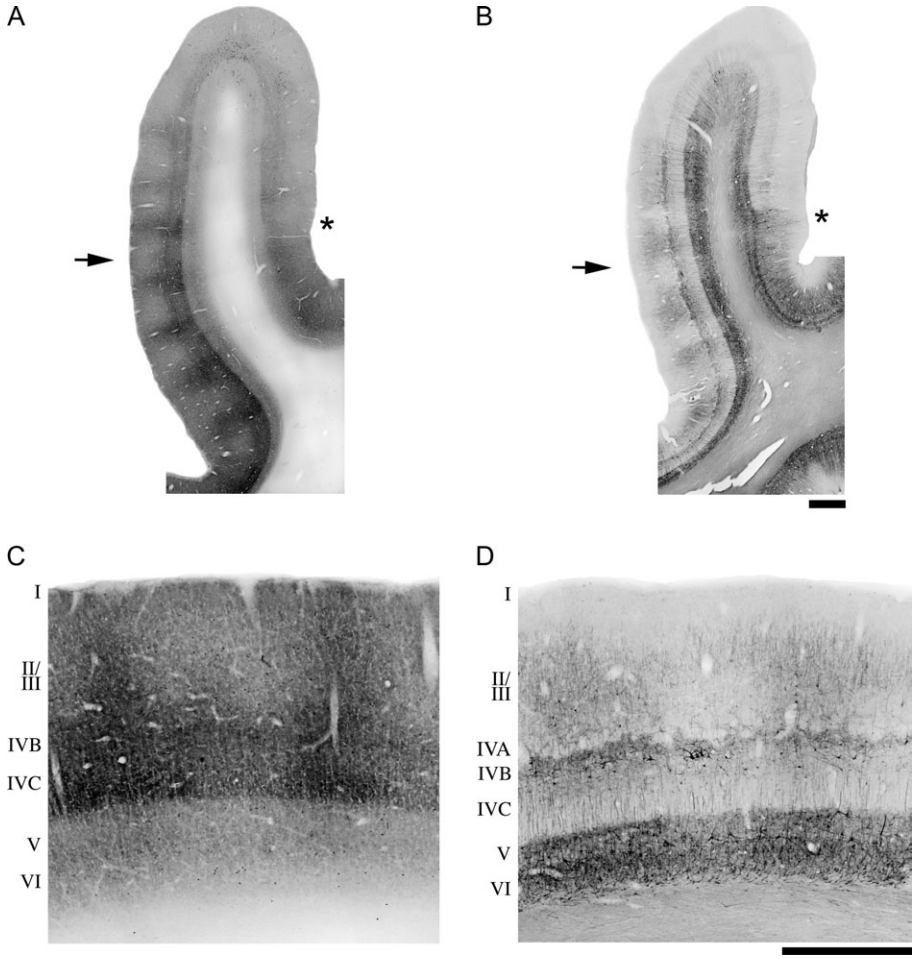

Figure 2. Low-magnification (top) and high-magnification (bottom) photomicrographs of nonadjacent coronal V1 sections through the posterior aspect of the cuneus revealed a distinct laminar pattern when stained for CO (*A*, *C*) or labeled for nonphosphorylated neurofilament (*B*, *D*). CO staining was found in all layers but was heaviest within layer IVC. Neurofilament labeling was strong in layers II/III, IVB, V, and VI, whereas layer IVC was weakly labeled. For both markers, alternating patches of dark and light reactivity were found within each layer of V1 and this pattern was aligned across layers. High-magnification photomicrographs (*C*, *D*) are from the regions in (*A*, *B*) that are highlighted with arrows. The asterisks in (*A*, *B*) identify the approximate V1/V2 boundary. This border was determined using area-specific anatomical characteristics that have been described in neurofilament-labeled sections from the human visual cortex (Hof and Morrison 1990). Scale bars = 1 mm.

below and adjacent to a neurofilament section where the labeling qualities identified it as having been cut through layer IVB. Although the characteristics of Nissl staining in this section were consistent with those typical of layer IVB, it is possible that a small portion of the ventral aspect of this section contained layer IVC cells. Measurements from deprived and nondeprived ocular dominance columns were taken from 5 sampling areas that were each approximately 9 mm^2. Only neurons with stained nucleoli were examined to ensure that measurements were consistently obtained from the midline of the cell body. Neurons were distinguished from glial cells using a high-power objective (20×) that revealed neurons by their distinct staining pattern, which included a visible cytoplasm, pale nucleus, and dark nucleolus. Cells exhibiting nuclear but not cytoplasmic staining (putative glial cells) were not included in the analysis. Statistical comparison across deprived and nondeprived ocular dominance columns was performed using a paired student's *t*-test.

CO blobs in layers II/III and ocular dominance columns in layer IVC were aligned for comparison using the pattern of radial blood vessels. Comparisons were calculated from 4 sampling regions that were each approximately 30 mm^2. CO blob and ocular dominance column borders were identified in an automated manner using a contour program. Ocular dominance column borders within layer IV were determined using the method described above. Contours representing between 50–60% of the maximum optical staining intensity within the analysis window were plotted to identify nondeprived and deprived CO blob borders (50%) in layers II/III, and blob centers were identified as the center of the contour representing 60% intensity within the program-defined blob border. The spatial relationship between blobs and ocular dominance columns was quantified by measuring the distance from each blob center to the nearest ocular dominance column border and dividing this number by half the width of the column at that location. This provided a metric ranging from 0 (border) to 1 (center) that determined each blob's position within an ocular dominance column. Results were analyzed using a chi-square test.

Results

Optic Nerves and Lateral Geniculate Nuclei

Histological processing of the subject's optic nerves and lateral geniculate nuclei provided supporting evidence of her reported monocular blindness. Examination of the optic nerves demonstrated that there was a substantial loss of myelinated fibers in the nerve associated with the deprived eye, whereas the degree of myelin staining in the other optic nerve was unremarkable (Fig. 1*A*,*B*). Examination of the lateral geniculate nuclei indicated that there was weak Nissl staining within deprived layers (Fig. 1*C*), and deprived neurons exhibited marked transsynaptic degeneration (Fig. 1*D*). This deprivation effect was

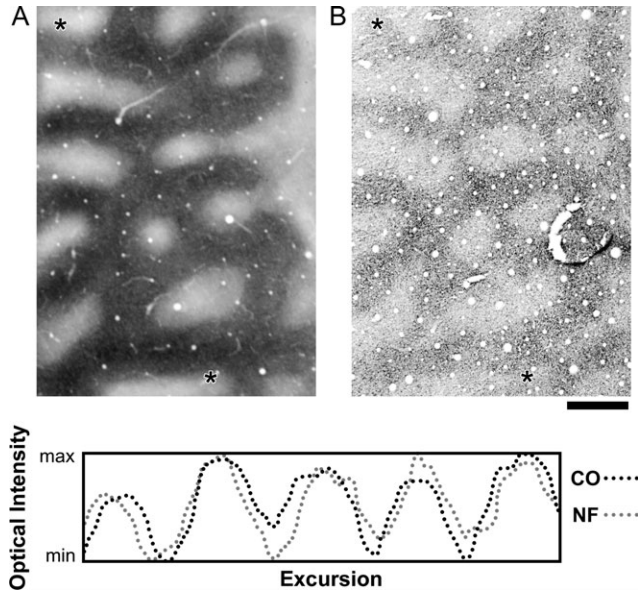

Figure 3. Sections cut tangential to the cortical surface revealed alternating dark and light regions of CO staining in layer IVC (*A*) and neurofilament labeling in layer IVB (*B*). These sections were aligned using the pattern of radial blood vessels, and the reaction patterns were compared by calculating optical profiles through the same regions in each section (along a line joining the 2 asterisks in *A* and *B*). The profiles for CO (black dotted line) and neurofilament (gray dotted line) showed substantial overlap ($r = 0.77$). Thus, the same regions of V1 have reduced CO staining and neurofilament labeling. Scale bar = 1 mm.

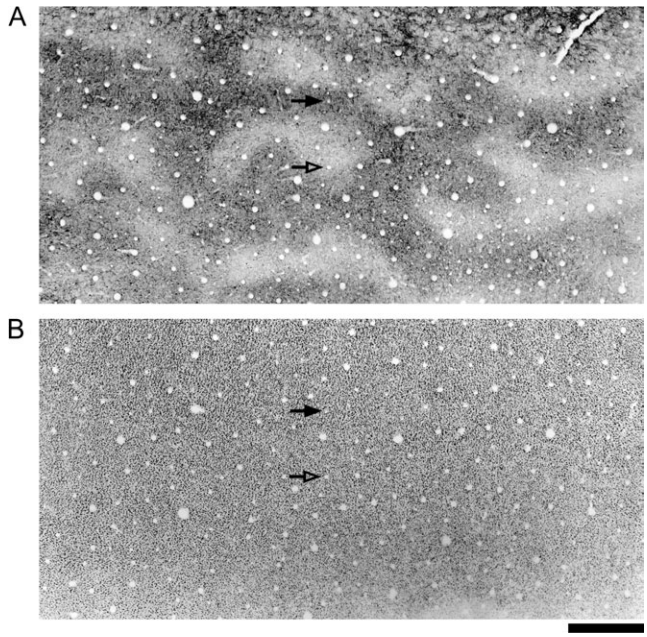

Figure 4. Adjacent sections cut tangentially and labeled for neurofilament (*A*) or stained for Nissl substance (*B*) were aligned for comparison using the pattern of radial blood vessels. The neurofilament section contained distinctly labeled multipolar cells that identified it as having been cut through layer IVB. Neurofilament labeling revealed a distinct pattern of ocular dominance that consisted of alternating regions of dark (nondeprived) and light (deprived) immunoreactivity. The adjacent section assessed for Nissl substance showed homogeneous staining at low magnification and did not exhibit an ocular dominance pattern. Arrows in this figure point to overlapping deprived (hollow arrows) and nondeprived (filled arrows) areas for the 2 markers. Scale bar = 1 mm.

best seen in the parvocellular layers corresponding to the deprived eye.

Primary Visual Cortex

Coronal sections of V1 that were reacted for CO or nonphosphorylated neurofilament showed distinct laminar patterns (Fig. 2). CO staining within layers II/III was nonuniformly distributed into alternating dark and light patches that were elongated perpendicular to the cortical surface (Fig. 2*A*). CO staining was heaviest within layer IVC where, as in the superficial layers, it was arranged into alternating dark and light patches (Fig. 2*C*). Layers V and VI were less intensely stained than the other layers but nevertheless also showed a low-contrast pattern of light and dark patches. The dark and light patches of CO staining from each layer within V1 were spatially aligned to form columns that were oriented perpendicular to the cortical surface and extended the full thickness of V1. It is worth mentioning that we were unable to identify a layer IVA in CO-stained sections. This finding supports previous research that was unable to identify layer IVA in human V1 using CO staining (Horton and Hedley-Whyte 1984; Wong-Riley and others 1993; Preuss and others 1999).

The distribution of nonphosphorylated neurofilament labeling (SMI-32) within the layers of V1 exhibited an obvious alternating pattern of dark and light patches that were oriented perpendicular to the cortical surface and appeared similar to the pattern of CO staining (Fig. 2*B*). Layer IVA was apparent with neurofilament labeling because it contained a pattern of clustered immunopositive somata and layer IVB processes, a labeling characteristic that has previously been shown to reliably identify human layer IVA (Yoshioka and Hendry 1995). Neurofilament immunoreactivity, which was primarily located within the soma and dendrites of pyramidal cells, showed strongest labeling in layers IVB, V, and VI, whereas layer IVC showed relatively weak labeling (Fig. 2*D*).

Sections of V1 cut in the tangential plane and stained for CO revealed a crisp pattern of alternating dark and light regions throughout layer IVC (Fig. 3*A*). In directly manipulated animal systems, previous studies have reported reduced CO staining in deprived-eye ocular dominance columns (Wong-Riley 1979; Horton 1984; Hendry and Jones 1986; Hendry and Bhandari 1992; Chaudhuri and others 1995; Horton and Hocking 1997, 1998). On this basis, we have interpreted the light regions of CO staining in layer IVC as marking ocular dominance columns serving the deprived eye. Despite the lengthy period of deprivation, the width of dark (mean = 645 μm, standard error of mean [SEM] = 95 μm) and light (mean = 600 μm, SEM = 59.5 μm) CO columns through layer IVC was not significantly different ($P = 0.27$), indicating that the deprivation did not produce substantial atrophy of deprived-eye columns.

A clear pattern of alternating dark and light regions was apparent in sections through layer IVB labeled for nonphosphorylated neurofilament (Fig. 3*B*). The tangential pattern of neurofilament labeling in layer IVB was similar to the pattern of CO staining in layer IVC. Optical intensity profiles calculated from the same location within CO and neurofilament sections indicated that the 2 patterns were correlated ($r = 0.77$; profiles in Fig. 3). Thus, neurons within the deprived-eye's ocular dominance columns showed a substantial reduction of neurofilament labeling. At the cellular level, the pattern of decreased immunoreactivity for neurofilament protein could be attributed

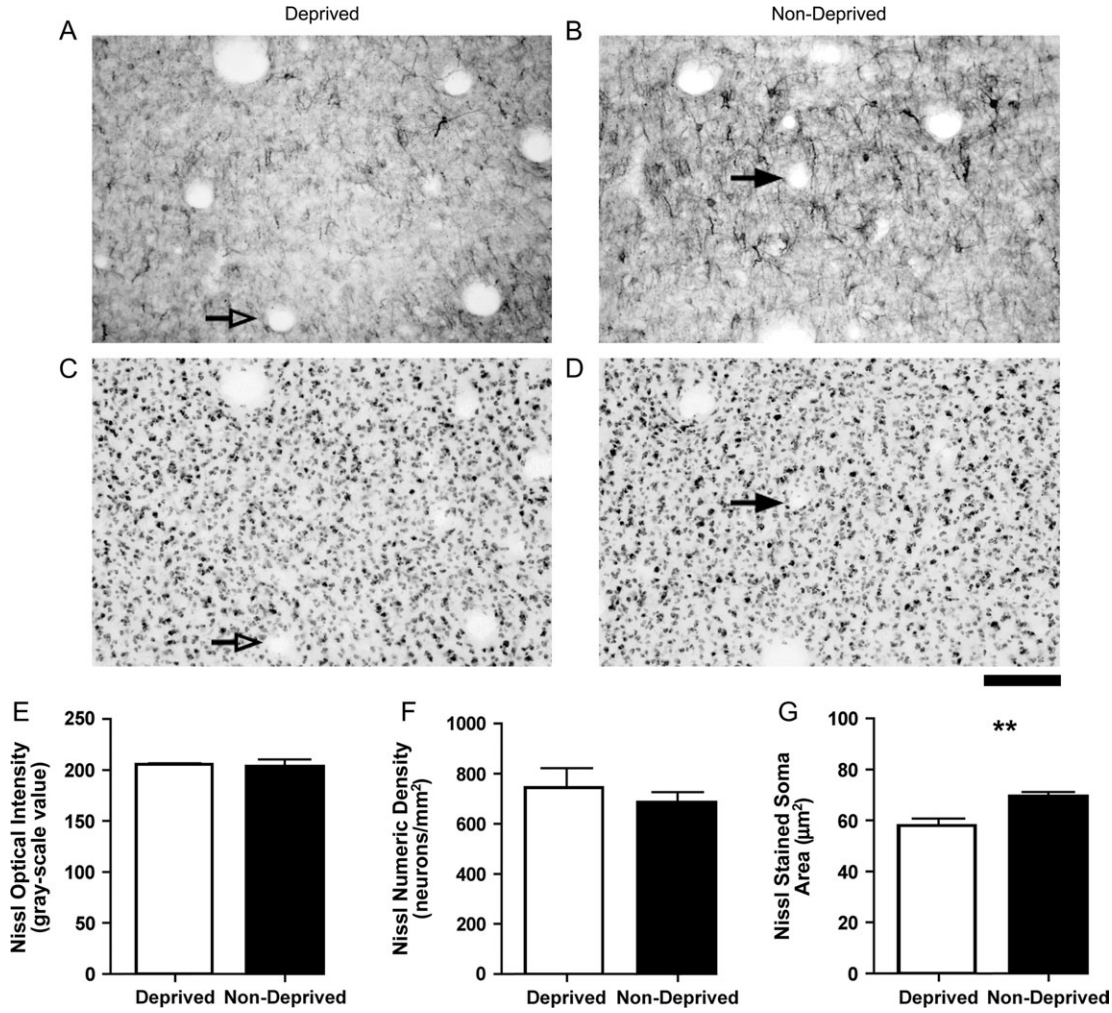

Figure 5. High-magnification photomicrographs of the regions highlighted with arrows in Figure 4. Significantly, fewer neurofilament-labeled somata and dendrites were found within parts of V1 serving the deprived eye (*A*) when compared with parts serving the nondeprived eye (*B*). No obvious difference in staining intensity between deprived and nondeprived areas was observed after Nissl staining (*C*, *D*). Quantification of staining intensity (*E*) and numeric density (*F*) showed no statistical difference between deprived and nondeprived regions ($P = 0.3$ and $P = 0.6$, respectively); however, the cross-sectional area of neuron somata (*G*) within deprived parts of V1 was significantly smaller than somata within nondeprived parts ($P = 0.02$). Arrows in this figure point to overlapping blood vessels between sections. Double asterisks indicate significant difference. Error bars represent SEM. Scale bar = 100 μm.

to a decrease in the density of neurofilament-labeled neurons within deprived-eye ocular dominance columns. The mean neurofilament-labeled neuron density within nondeprived ocular dominance columns was 37 neurons/mm^2 (SEM = 4.5 neurons/mm^2), whereas the density within deprived columns was significantly reduced ($P = 0.014$) to 9 neurons/mm^2 (SEM 2.0 neurons/mm^2).

An examination of Nissl staining was performed to determine if the decrease in neurofilament labeling was due to a loss of neurons within deprived regions of V1 (Fig. 4). Although a tangentially cut section through layer IVB labeled for neurofilament showed a crisp pattern of ocular dominance columns (Fig. 4*A*), we could not identify an ocular dominance pattern in an adjacent Nissl-stained section (Fig. 4*B*) or from Nissl sections cut through other layers of V1. Photomicrographs of the deprived and nondeprived regions highlighted with arrows in Figure 4 show reduced neurofilament labeling in deprived territory (Fig. 5*A*,*B*) without an apparent loss of Nissl staining (Fig. 5*C*,*D*). Quantification of Nissl staining intensity (Fig. 5*E*) and density of Nissl-stained neurons (Fig. 5*F*) revealed that there were no statistically significant differences between deprived and nondeprived regions. Analysis of soma area (Fig. 5*G*) indicated that neuronal somata located within deprived areas of V1 were significantly smaller (16%) than somata in nondeprived areas ($P = 0.022$). Nissl-stained neurons in deprived-eye columns had an average soma size of 58 μm^2 (SEM = 3.4 μm^2), whereas nondeprived somata were, on average, 69 μm^2 (SEM = 1.2 μm^2).

Characteristics of the tangential pattern of CO staining and neurofilament labeling varied at different depths through the cortex (Fig. 6). In the superficial layers, CO staining was arranged into a pattern of dark blobs that were often linked together by lighter bands of staining (Fig. 6*A*). When aligned with the ocular dominance pattern from layer IVC, it was clear that the linked blobs were located within the borders of nondeprived ocular dominance columns. Blobs that aligned with deprived-eye columns were often isolated and less densely stained compared with nondeprived blobs. In some parts of V1, blobs could barely be detected within deprived columns. An adjacent section through the superficial layers labeled for

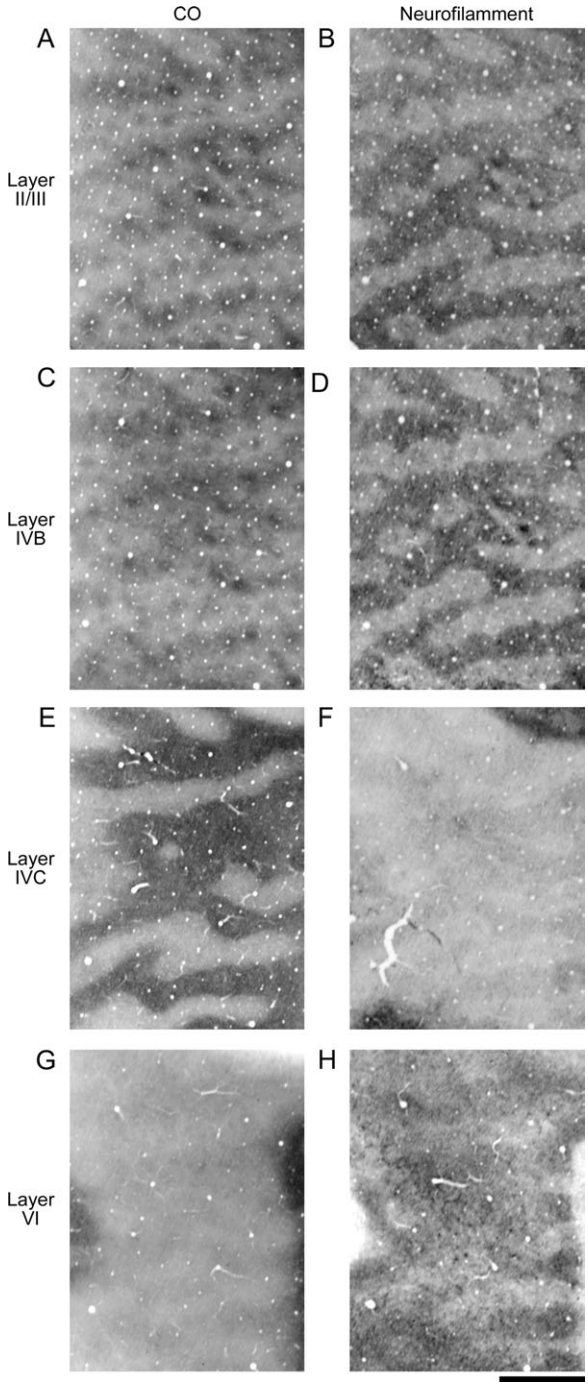

Figure 6. This figure shows a series of adjacent sections at different depths through V1 that were reacted for either CO (left) or neurofilament (right). Sections through layer II/III (*A*) and IVB (*C*) that were reacted for CO showed regularly spaced blobs of reactivity. A bridge of pale reactivity connected darkly stained CO blobs within nondeprived ocular dominance columns, whereas blobs in deprived columns were often isolated and stained less intensely. Neurofilament labeling within layers II/III (*B*) and layer IVB (*D*) was organized into alternating dark and light regions. Layer IVC showed strong reactivity for CO but was weakly labeled for neurofilament (*E*, *F*). CO staining within layer IVC (*E*) was organized into distinct dark and light areas that aligned with the pattern of CO staining and neurofilament labeling in the more superficial layers. Neurofilament labeling in layer IVC was weak and revealed only a faint ocular dominance pattern (*F*). Sections through layer VI were lightly stained for CO and showed a weak ocular dominance pattern (*G*). Neurofilament labeling in layer VI was heavy and showed a low-contrast ocular dominance pattern (*H*). Scale bar = 2 mm.

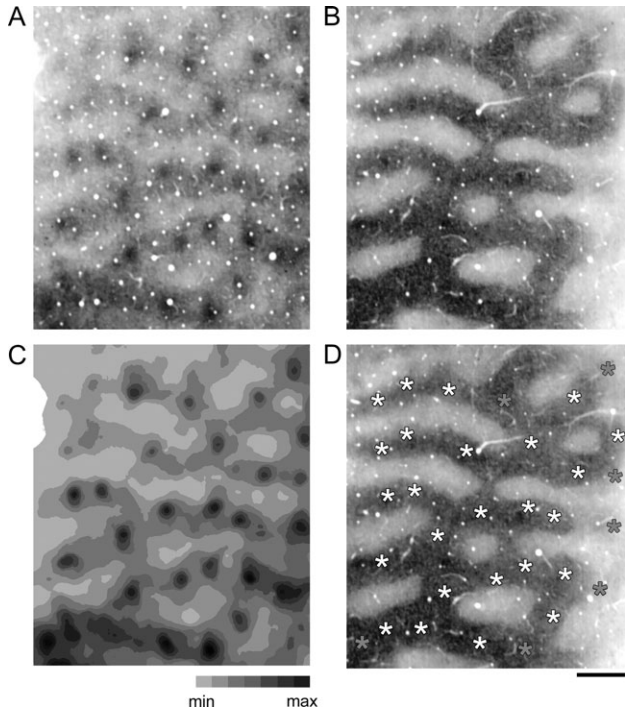

Figure 7. The spatial relationship between CO blobs and ocular dominance columns is demonstrated in this figure. A section through the superficial layers that contained CO blobs (*A*) was aligned with a section through layer IVC that contained a pattern of ocular dominance columns (*B*). Blobs were identified using an automated computer program that calculated relative optical densities throughout the section (*C*) and then plotted filled contours representing maximum-to-minimum staining intensities across the section. Markers (asterisks) representing computer-identified blob centers (max staining) were aligned with the map of ocular dominance, and then blob position within the map was evaluated. The gray asterisks in (*D*) represent blobs that could not be related to ocular dominance columns because surrounding column borders were not clear. Scale bar = 1 mm.

neurofilament protein showed a crisp pattern of alternating dark and light regions that, at a microscopic scale, were composed of labeled cell bodies and dendrites (Fig. 6*B*). Layer IVB showed a similar pattern of results for both markers (Fig. 6*C*,*D*) with the exception that the neurofilament-labeled ocular dominance pattern was more distinct in layer IVB compared with that found in the superficial layers. CO staining within layer IVC was strong and segregated into crisp alternating dark and light regions that aligned with the more superficial patterns found for both CO and neurofilament (Fig. 6*E*). Overall neurofilament labeling within layer IVC was weak, but a low-contrast ocular dominance pattern was still observed because of labeled apical dendrite shafts originating from layer V and VI cells (Fig. 6*F*). Infragranular layers were less densely stained for CO compared with layer IVC, and there was a comparatively less obvious ocular dominance pattern (Fig. 6*G*). The adjacent neurofilament section was darkly labeled and contained low-contrast dark and light regions that aligned with those found in superficial parts of V1 (Fig. 6*H*). Although CO and neurofilament reactivity showed some variability between layers, the ocular dominance pattern found within the layers overlapped for both markers.

Alignment of Blobs and Ocular Dominance Columns

A previous study demonstrated that human CO blobs are eye-specific (Horton and Hedley-Whyte 1984); however, the extent to which the human blobs (nondeprived and deprived) align

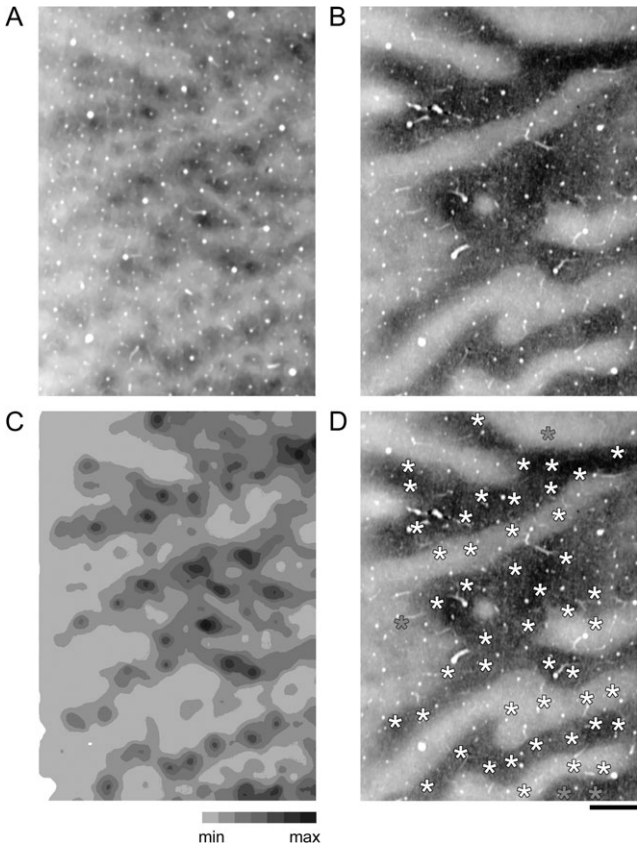

Figure 8. This figure shows an example of the spatial relationship between blobs within the superficial layers (*A*) and ocular dominance columns in layer IVC (*B*) taken from a different region of V1. CO blobs were identified using a computer program that plotted filled contours representing maximum-to-minimum staining intensities (*C*), and an asterisk was positioned at the center of each computer-identified blob (*D*). The asterisks representing blobs were spatially aligned with the ocular dominance map to examine the relationship between these 2 features. The gray asterisks in (*D*) represent blobs that could not be evaluated because of unclear ocular dominance borders. Scale bar = 1 mm.

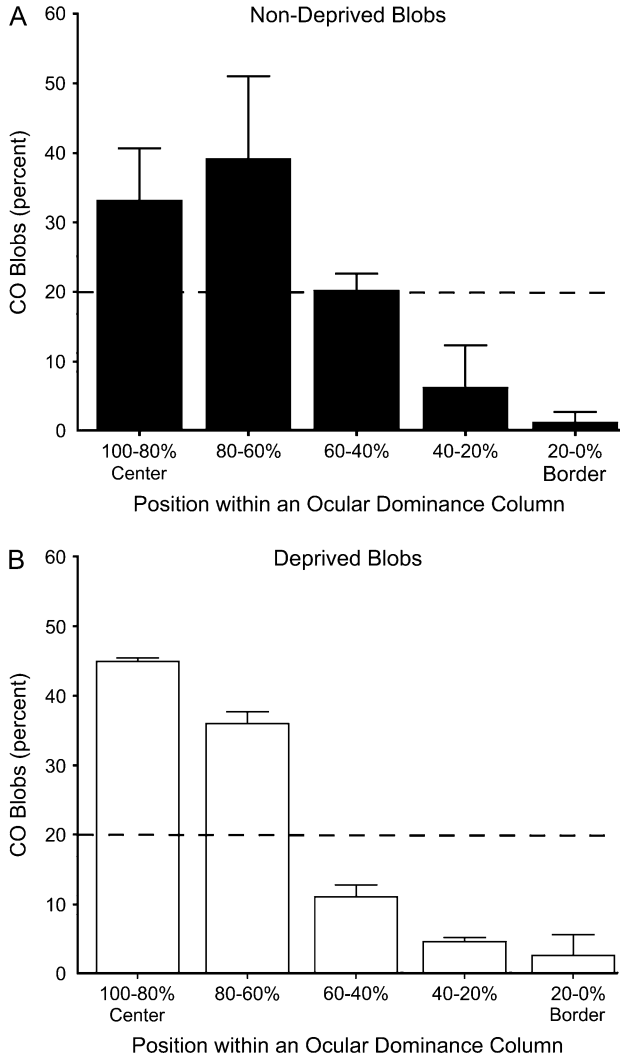

Figure 9. Quantification of the spatial relationship between CO blobs and ocular dominance columns. These graphs plot the distribution of nondeprived (*A*) and deprived (*B*) blob position within an ocular dominance column, from the center of a column to the border. The distance from the center of a blob to the nearest column border was calculated and divided by half of the total column width at that position. This provided a number that ranged from 1, for blobs aligned with the center of an ocular dominance column, to 0, for blobs aligned with a border. The distribution of positional measurements for both nondeprived and deprived blobs was skewed to the left, indicating that the majority of blobs were located near the center of an ocular dominance column and few were positioned along a border. A chi-square statistic revealed that the distribution of deprived and nondeprived blobs was significantly different from that expected by a random distribution ($P < 0.0001$). The dashed line represents the blob percentage for each column position that would be expected if blobs were randomly distributed across the ocular dominance map. Error bars represent standard deviation.

with the centers of ocular dominance columns was not quantified. The crisp patterns of CO blobs and ocular dominance columns that were obtained from V1 in this study enabled a quantification of the spatial layout of blobs with respect to ocular dominance columns (Figs 7 and 8). CO blobs in superficial layers of V1 were identified using an automated method that determined the location of blob centers, which were then aligned with a computer-defined ocular dominance pattern derived from CO sections through layer IVC (see Materials and Methods). The distribution of nondeprived (n = 91) and deprived (n = 43) blobs relative to ocular dominance column borders (Fig. 9) demonstrated that the majority of blobs (>70%) were positioned near the center of ocular dominance columns, and few blobs (<10%) were located near borders. This spatial relationship was statistically different from a random distribution for blobs located within both deprived (chi-square $P < 0.0001$) and nondeprived (chi-square $P < 0.0001$) ocular dominance columns.

Discussion

The results of this study demonstrate that long-term monocular deprivation has a profound impact on CO staining and neurofilament labeling in human V1. Using CO histochemistry to reveal the pattern of ocular dominance, we found a significant loss of neurofilament labeling within the deprived-eye's ocular dominance columns, despite preservation of column width. The loss was greatest in the superficial layers and within layer IVB, while a less obvious reduction was observed within layers V and VI. The average cross-sectional area of neurons was found to be significantly smaller in deprived regions of V1 when compared with nondeprived regions. Quantification of the spatial relationship between CO blobs and ocular dominance columns revealed that, like the macaque monkey, human blobs tend to be positioned along the center of ocular dominance columns.

The impact of visual deprivation on human V1 has previously been examined in subjects whose deprivation was induced by monocular enucleation (Horton and Hedley-Whyte 1984). Although the subject in our study had both eyes intact at the time of death, some of the results we obtained from her visual cortex are in agreement with the findings of Horton and Hedley-Whyte (1984). In both studies, ocular dominance columns in V1 were revealed by reduced CO staining within deprived-eye columns, and although there was not pronounced shrinkage of columns reported in either study, both found that cells within deprived columns were comparatively smaller than those within nondeprived columns, by 10% after enucleation and by 16% in our study. Unlike Horton and Hedley-Whyte (1984), we did not observe darker Nissl staining or increased neuronal packing within deprived-eye columns. The source of this discrepancy is not clear, but it suggests that our subject's deprivation was not equivalent to monocular enucleation.

In monkey V1, monocular deprivation early in life causes a loss of neurofilament labeling within deprived-eye ocular dominance columns that is not found when deprivation is initiated in adulthood (Duffy and Livingstone 2005). The loss of neurofilament protein after early monocular deprivation was suggested to be involved in the restructuring of neural connections that result when deprivation is begun during the highly plastic sensitive period. We do not believe that the loss of neurofilament within human V1 that we report in this study represents an active restructuring of neural connections within deprived-eye columns because extensive reorganization would likely have taken place during early development. The loss of neurofilament labeling within deprived V1 neurons may represent a homeostatic downregulation in response to a reduced level of activity brought about by the long-standing visual deprivation. It is also possible that reduced neurofilament reactivity resulted from secondary transneuronal degeneration, of the type described by Horton and Hedley-Whyte (1984) in human enucleates. This latter notion is supported by our direct observation of the deprived optic nerve and the deprived layers of lateral geniculate nuclei, which both showed degenerative hallmarks such as loss of myelin and neural atrophy.

Monocular lid suture in macaque monkeys produces substantial shrinkage of deprived ocular dominance columns only when deprivation is initiated in early development (LeVay and others 1980; Horton and Hocking 1997). In human V1, monocular enucleation during the first week of life results in homogenous CO staining in layer IVC that is likely the consequence of complete dominance by the intact eye (Horton and Hocking 1998). That V1 from the subject in this study did not exhibit a shrinkage of ocular dominance columns suggests either that her monocular impairment was present during early life, but was not sufficient to induce reorganization of ocular dominance, or that the impairment developed beyond the sensitive period for ocular dominance plasticity. Despite the absence of an ocular dominance shift, the long-standing deprivation was severe enough to produce substantial anatomical change in the optic nerve, lateral geniculate nuclei, and V1. Thus, pronounced anatomical changes induced by monocular deprivation may not necessarily be accompanied by a shift in ocular dominance columns. This is similar to a previous study of human V1 where a long-standing amblyopia did not produce a change in ocular dominance column width (Horton and Stryker 1993).

The spatial relationship between CO blobs and ocular dominance columns has been investigated in nonhuman primates (Horton and Hubel 1981; Horton 1984; Horton and Hocking 1996; Xu and others 2005) and cats (Murphy and others 1995). The results from those studies revealed a high degree of variability across species. In macaque monkey, CO blobs are confined within the borders of ocular dominance columns and are spatially aligned with column centers (Horton and Hubel 1981; Horton 1984). In squirrel monkey and galago, there is not a consistent spatial relationship between blobs and columns (Horton and Hocking 1996; Xu and others 2005). CO blobs in cat V1 are similar to the macaque in that they are also found over each eye's ocular dominance columns; however, the positioning of blobs within columns is not as precise (Murphy and others 1995). In this study, we have demonstrated quantitatively that the vast majority of CO blobs in human V1 spatially align with the centers of ocular dominance columns. We found this to be true for blobs positioned within deprived and nondeprived columns. Although the extent to which this result translates to the normal condition remains unknown, it suggests that the organization of human blobs is more similar to that of macaque monkey than to other species within which this issue has been investigated. In the macaque monkey, lateral geniculate nucleus inputs to the superficial layers of V1 are clustered into patches that overlap with CO blobs (Livingstone and Hubel 1982). The similar organization between human and macaque V1 raises the possibility that the arrangement of lateral geniculate nucleus inputs to the superficial layers of human V1 is patchy and aligned with CO blobs. Finally, the spatial positioning of blobs was the same in deprived- and nondeprived-eye columns, suggesting that the arrangement of these features in human V1 is independent of visual experience.

Notes

This work was supported by grants from the National Eye Institute (EY13135 and EY16187) to MSL and the Natural Sciences and Engineering Research Council of Canada to KRD. The authors thank Donald Mitchell for helpful comments on the manuscript. *Conflict of Interest*: None declared.

Address correspondence to email: kevin.duffy@dal.ca.

References

Bickford ME, Guido W, Godwin DW. 1998. Neurofilament proteins in Y-cells of the cat lateral geniculate nucleus: normal expression and alteration with visual deprivation. J Neurosci 18:6549–6557.

Carroll EW, Wong-Riley MT. 1984. Quantitative light and electron microscopic analysis of cytochrome oxidase-rich zone in the striate cortex of the squirrel monkey. J Comp Neurol 222:1–17.

Chaudhuri A, Matsubara JA, Cynader MS. 1995. Neuronal activity in primate visual cortex assessed by immunostaining for the transcription factor Zif268. Vis Neurosci 12:35–50.

DeYoe EA, Trusk TC, Wong-Riley MT. 1995. Activity correlates of cytochrome oxidase-defined compartments in granular and supragranular layers of primary visual cortex of the macaque monkey. Vis Neurosci 12:629–639.

Duffy KR, Livingstone MS. 2005. Loss of neurofilament labeling in the primary visual cortex of monocularly deprived monkeys. Cereb Cortex 15:1146–1154.

Hendry SH, Bhandari MA. 1992. Neuronal organization and plasticity in adult monkey visual cortex: immunoreactivity for microtubule-associated protein 2. Vis Neurosci 9:445–459.

Hendry SH, Jones EG. 1986. Reduction in number of immunostained GABAergic neurons in deprived-eye dominance columns of monkey area 17. Nature 320:750–752.

Hof PR, Morrison JH. 1990. Quantitative analysis of a vulnerable subset of pyramidal neurons in Alzheimer's disease: II. Primary and secondary visual cortex. J Comp Neurol 301:55–64.
Horton JC. 1984. Cytochrome oxidase patches: a new cytoarchitectonic feature of monkey visual cortex. Philos Trans R Soc Lond B Biol Sci 304:199–253.
Horton JC, Hedley-Whyte ET. 1984. Mapping of cytochrome oxidase patches and ocular dominance columns in human visual cortex. Philos Trans R Soc Lond B 304:255–272.
Horton JC, Hocking DR. 1996. Anatomical demonstration of ocular dominance columns in striate cortex of the squirrel monkey. J Neurosci 16:5510–5522.
Horton JC, Hocking DR. 1997. Timing of the critical period for plasticity of ocular dominance columns in macaque striate cortex. J Neurosci 17:3684–3709.
Horton JC, Hocking DR. 1998. Effect of early monocular enucleation upon ocular dominance columns and cytochrome oxidase activity in monkey and human visual cortex. Vis Neurosci 15:289–303.
Horton JC, Hubel DH. 1981. Regular patchy distribution of cytochrome oxidase staining in primary visual cortex of macaque monkey. Nature 292:762–764.
Horton JC, Stryker MP. 1993. Amblyopia induced by anisometropia without shrinkage of ocular dominance columns in human striate cortex. Proc Natl Acad Sci USA 90:5494–5498.
Hubel DH, Wiesel TN. 1959. Single unit activity in striate cortex of unrestrained cats. J Physiol 147:226–238.
Hubel DH, Wiesel TN. 1962. Receptive fields, inocular interaction and functional architecture in the cat's visual cortex. J Physiol 160:106–154.
Hubel DH, Wiesel TN. 1968. Receptive fields and functional architecture of monkey striate cortex. J Physiol 195:215–243.
Hubel DH, Wiesel TN. 1972. Laminar and columnar distribution of geniculo-cortical fibers in the macaque monkey. J Comp Neurol 146:421–450.
Lee VM, Otvos YL, Carden MJ, Hollosi M, Dietzschold B, Lazzarini RA. 1988. Identification of the major multiphosphorylation site in mammalian neurofilaments. Proc Natl Acad Sci USA 85: 1998–2002.
LeVay S, Hubel DH, Wiesel TN. 1975. The pattern of ocular dominance columns in macaque visual cortex revealed by a reduced silver stain. J Comp Neurol 159:559–576.
LeVay S, Wiesel TN, Hubel DH. 1980. The development of ocular dominance columns in normal and visually deprived monkeys. J Comp Neurol 191:1–51.
Livingstone MS, Hubel DH. 1982. Thalamic inputs to cytochrome oxidase-rich regions in monkey visual cortex. Proc Natl Acad Sci USA 79:6098–6101.
Livingstone MS, Hubel DH. 1984. Anatomy and physiology of a color system in the primate visual cortex. J Neurosci 4:309–356.
Murphy KM, Jones DG, Van Sluyters RC. 1995. Cytochrome-oxidase blobs in cat primary visual cortex. J Neurosci 15:4196–4208.
Preuss TM, Huixin QI, Kaas JH. 1999. Distinctive compartmentalization of human primary visual cortex. Proc Natl Acad Sci USA 96:11601–11606.
Wong-Riley MTT. 1979. Changes in the visual system of monocularly sutured or enucleated cat demonstrable with cytochrome oxidase histochemistry. Brain Res 171:11–28.
Wong-Riley MTT, Hevner RF, Cutlan R, Earnest M, Egan R, Frost J, Nguyen T. 1993. Cytochrome oxidase in the human visual cortex: distribution in the developing and adult brain. Vis Neurosci 10:41–58.
Xu X, Bosking WH, White LE, Fitzpatrick D, Casagrande VA. 2005. Functional organization of visual cortex in the prosimian bush baby revealed by optical imaging of intrinsic signals. J Neurophysiol 94: 2748–2762.
Yoshioka T, Hendry SH. 1995. Compartmental organization of layer IVA in human primary visual cortex. J Comp Neurol 359:213–220.